SF 298 MASTER COPY KEEP THIS COPY FOR REPRODUCTION PURPOSES

REPORT DOCUMENTATION PAGE

Form Approved
OMB NO. 0704-0188

1. AGENCY USE ONLY *(Leave blank)*	2. REPORT DATE	3. REPORT TYPE AND DATES COVERED
	July 23, 1996	

4. TITLE AND SUBTITLE
Development of a Reduced Chemical Kinetic Model for Prediction of Preignition Reactivity and Autoignition of Primary Reference Fuels

5. FUNDING NUMBERS
DAAH04-93-G-0042

6. AUTHOR(S)
Houliang Li; David L. Miller; Nicholas P. Cernansky

7. PERFORMING ORGANIZATION NAMES(S) AND ADDRESS(ES)
Drexel University
Mechanical Engineering
32nd and Chestnut Streets
Philadelphia, PA 19104

8. PERFORMING ORGANIZATION REPORT NUMBER

9. SPONSORING / MONITORING AGENCY NAME(S) AND ADDRESS(ES)
U.S. Army Research Office
P.O. Box 12211
Research Triangle Park, NC 27709-2211

10. SPONSORING / MONITORING AGENCY REPORT NUMBER
ARO 30782.8-EG

11. SUPPLEMENTARY NOTES
The views, opinions and/or findings contained in this report are those of the author(s) and should not be construed as an official Department of the Army position, policy or decision, unless so designated by other documentation.

12a. DISTRIBUTION / AVAILABILITY STATEMENT
Approved for public release; distribution unlimited.

13. ABSTRACT *(Maximum 200 words)*
A reduced chemical kinetic model has been developed for the prediction of major oxidation behavior of primary reference fuels (PRF's) in a motored engine, including ignition delay preignition heat release, fuel consumption, CO formation and production of other species classes. This model consists of 29 reactions with 20 active species and was tuned to be applicable for the neat PRF's, 87 PRF and 63 PRF, and at various engine conditions. At the motored engine condition where detailed species data were generated, the model reproduces the ignition delay and the preignition heat release quite well (to within 15%). Fuel consumption and CO formation predictions differed from experiments by at most 25% for all of the four fuels. Predictions for other species classes generally agreed with experiments. As inlet temperature was varied, the experimentally observed negative temperature coefficient (NTC) behavior of iso-octane and 87 PRF was reproduced by the model. In addtion, the lower reactivity of 87 PRF at a lower compression ratio was also predicted, indicating that the model can account for the effects of pressure or charge density.

14. SUBJECT TERMS	15. NUMBER IF PAGES
Primary Reference Fuels, Reduced Kinetic Model, Preignition Chemistry, Autoignition, Engine Combustion	16. PRICE CODE

17. SECURITY CLASSIFICATION OR REPORT	18. SECURITY CLASSIFICATION OF THIS PAGE	19. SECURITY CLASSIFICATION OF ABSTRACT	20. LIMITATION OF ABSTRACT
UNCLASSIFIED	UNCLASSIFIED	UNCLASSIFIED	UL

GENERAL INSTRUCTIONS FOR COMPLETING SF 298

The Report Documentation Page (RDP) is used in announcing and cataloging reports. It is important that this information be consistent with the rest of the report, particularly the cover and title page. instructions for filling in each block of the form follow. It is important to ***stay within the lines*** to meet ***optical scanning requirements.***

Block 1. Agency Use Only *(Leave blank)*

Block 2. Report Date. Full publication date including day, month, and year, if available (e.g. 1 Jan 88). Must cite at least year.

Block 3. Type of Report and Dates Covered. State whether report is interim, final, etc. If applicable, enter inclusive report dates (e.g. 10 Jun 87 - 30 Jun 88).

Block 4. Title and Subtitle. A title is taken from the part of the report that provides the most meaningful and complete information. When a report is prepared in more than one volume, repeat the primary title, add volume number, and include subtitle for the specific volume. On classified documents enter the title classification in parentheses.

Block 5. Funding Numbers. To include contract and grant numbers; may include program element number(s), project number(s), task number(s), and work unit number(s). Use the following labels:

C	- Contract	**PR**	- Project
G	- Grant	**TA**	- Task
PE	- Program Element	**WU**	- Work Unit Accession No.

Block 6. Author(s). Name(s) of person(s) responsible for writing the report, performing the research, or credited with the content of the report. If editor or compiler, this should follow the name(s).

Block 7. Performing Organization Name(s) and Address(es). Self-explanatory.

Block 8. Performing Organization Report Number. Enter the unique alphanumeric report number(s) assigned by the organization performing the report.

Block 9. Sponsoring/Monitoring Agency Name(s) and Address(es). Self-explanatory.

Block 10. Sponsoring/Monitoring Agency Report Number. *(If known)*

Block 11. Supplementary Notes. Enter information not included elsewhere such as; prepared in cooperation with...; Trans. of...; To be published in.... When a report is revised, include a statement whether the new report supersedes or supplements the older report.

Block 12a. Distribution/Availability Statement. Denotes public availability or limitations. Cite any availability to the public. Enter additional limitations or special markings in all capitals (e.g. NORFORN, REL, ITAR).

DOD	- See DoDD 4230.25, "Distribution Statements on Technical Documents."
DOE	- See authorities.
NASA	- See Handbook NHB 2200.2.
NTIS	- Leave blank.

Block 12b. Distribution Code.

DOD	- Leave blank
DOE	- Enter DOE distribution categories from the Standard Distribution for Unclassified Scientific and Technical Reports
NASA	- Leave blank.
NTIS	- Leave blank.

Block 13. Abstract. Include a brief *(Maximum 200 words)* factual summary of the most significant information contained in the report.

Block 14. Subject Terms. Keywords or phrases identifying major subjects in the report.

Block 15. Number of Pages. Enter the total number of pages.

Block 16. Price Code. Enter appropriate price code *(NTIS only).*

Block 17. - 19. Security Classifications. Self-explanatory. Enter U.S. Security Classification in accordance with U.S. Security Regulations (i.e., UNCLASSIFIED). If form contains classified information, stamp classification on the top and bottom of the page.

Block 20. Limitation of Abstract. This block must be completed to assign a limitation to the abstract. Enter either UL (unlimited) or SAR (same as report). An entry in this block is necessary if the abstract is to be limited. If blank, the abstract is assumed to be unlimited.

SAE TECHNICAL
PAPER SERIES

960498

Development of a Reduced Chemical Kinetic Model for Prediction of Preignition Reactivity and Autoignition of Primary Reference Fuels

Houliang Li, David L. Miller, and Nicholas P. Cernansky
Drexel Univ.

SAE The Engineering Society For Advancing Mobility Land Sea Air and Space®
INTERNATIONAL

International Congress & Exposition
Detroit, Michigan
February 26-29, 1996

400 Commonwealth Drive, Warrendale, PA 15096-0001 U.S.A. Tel: (412)776-4841 Fax:(412)776-5760

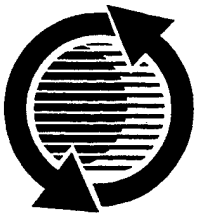

ISSN 0148-7191

Printed in USA 96-0049

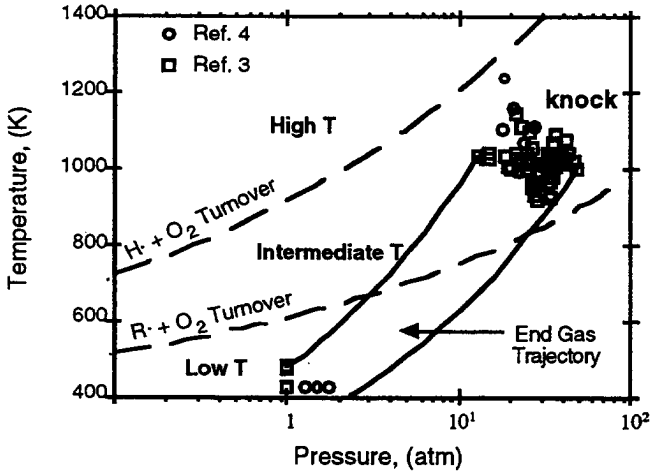

Figure 1. Typical SI engine envelope of gas temperature and pressure histories leading up to the point of knock.

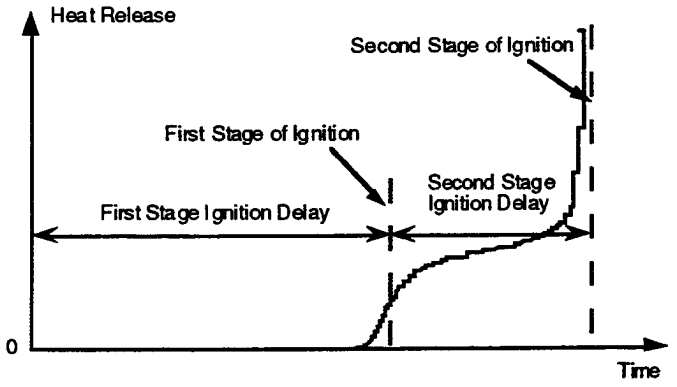

Figure 2. A typical heat release profile during a two stage ignition process.

[5]. Consequently, existing reduced models relevant to autoignition and engine knock [6-10] have been built up from skeleton reaction schemes in a rather empirical manner to include representative kinetic steps, which can be generic, global or elementary reactions. Instead of pursuing the details of oxidation chemistry, these models have been developed for prediction of overall ignition behavior. For paraffins larger than C3, a typical autoignition process occurs in two stages characterized by heat release as in Figure 2. This typical two stage ignition characteristic can be reproduced by the reduced models. Key rate parameters are generally derived by matching experimental results (historically ignition delays) which are measured in idealized facilities such as rapid compression machines and constant volume vessels.

While the reduced models correctly reproduced the overall trend of ignition delays as a function of reaction conditions (temperature, pressure, and reactant concentration) and fuel structure, significant quantitative discrepancies remain between the model prediction and experimental results. Further, the empiricism involved in these models can limit the scope of their applications. To enhance their predictive capability, reduced models should be validated against more detailed information on preignition behavior and under conditions as broad and varied as possible.

The important information on preignition behavior that has been overlooked in existing models includes the preignition heat release and evolution of chemical species. Experiments have shown that preignition reactions can significantly increase the temperature of end gases in SI engines [3,11]. Further, the preignition heat release has a complex dependence with reaction conditions, especially the temperature [12,13]. Thus, accounting for preignition heat release is important in reduced models in order to enhance their predictive ability under broad reaction conditions. Historically, reduced models have not been validated for species prediction and do not perform well in this regard. It is highly desirable that reduced models also have the ability to predict at least key chemical species or species classes, so that they can be linked and tuned with measured species data to better represent the key chemical processes

The objective of the current study is to develop a reduced chemical kinetic model capable of predicting the preignition heat release and key chemical species including fuel consumption, formation of a major oxidation product, CO, and production of other species classes, as well as ignition delays at low and intermediate temperatures. This work is a continuation of our previous effort in which we extended an existing reduced ignition model [9] to improve its prediction of preignition heat release and fuel consumption, and built in a new capacity for prediction of CO formation [14]. This extended model was tuned to match our experimental results with a 63 octane blend of PRF's, 63 PRF, in a motored engine at one operating condition. In the current work, we modified this extended model using experimental data from our recent motored engine study of n-heptane, iso-octane and 87 PRF [15]. Modifications were made to improve its prediction of preignition heat release, fuel consumption, and CO formation and to account for production of other species classes. The current model was tuned to be applicable for the neat PRF's, 87 PRF and 63 PRF, and at various engine conditions.

The initial model which we extended in our prior work [14] is reviewed next, followed by a detailed description of the current modified model. Results of predictions using the current model are then presented and discussed. Finally, a brief discussion of the status of this model is provided.

OVERVIEW OF PREVIOUS MODEL

In our previous work [14], we investigated the ability of an existing model of 18 reactions and 13 active species [9] to predict heat release and fuel consumption during the preignition reaction of 63 PRF in a motored research engine. The baseline model is listed in part I of Table 1, where RH represents the fuel. Given the initial fuel-air mixture concentration and temperature, the chemical kinetic model is used to predict temperature, heat release and species concentrations as a function of time or crank angle by integrating the coupled rate and energy equations. For comparison, we independently

calculated heat release from measured pressure data using a standard thermodynamic model.

We found that: (i) the induction time of heat release can be matched when the rate parameters of the alkylperoxide radical ($RO_2\cdot$) isomerization reaction are chosen between the values suggested for iso-octane and n-heptane; (ii) the heat release predicted by the kinetic model is about 20% lower than that calculated from the pressure data; and (iii) the model predicted a 100% fuel consumption while the measured fuel consumption is less than 50%. Analysis of the baseline model showed that in its present form, the specific heat release could not be matched.

This model was extended by adding 11 reactions and 7 active species to account for the oxidation of aldehydes (RCHO), olefins (C=C), carbonyl radicals (O=R·), and to build in a new capacity for the prediction of CO formation. These reactions are listed in Part II of Table 1. The heat release, fuel consumption and CO formation as a function of crank angle degree (CAD) predicted by the extended model, along with the predictions by the baseline model and experimental results, are presented in Figure 3.

The results show that the extended model significantly improved the prediction of heat release and fuel consumption. In addition, the extended model predicted CO formation reasonably well. However, in spite of these advances, further model enhancements obviously were necessary to improve these predictions, and to allow for predictions of other species classes. Since our recent experimental study [15] provided detailed species information for n-heptane, iso-octane and 87 PRF, the model was modified and adapted for these fuels. The final version of the model was also validated against the experimental results of 63 PRF presented in Figure 3.

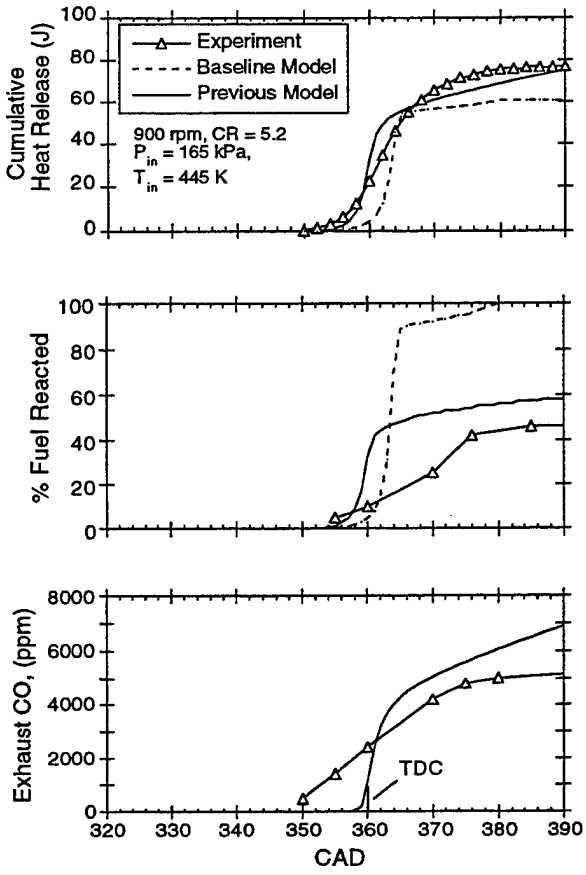

Figure 3. Comparison of the heat release, fuel consumption and exhaust CO predictions of our previous model, along with the predictions by the baseline model and the experimental results with 63 PRF [14].

RECENT MODEL MODIFICATIONS

In our recent motored engine study of autoignition chemistry of PRF's, we mapped the overall preignition reactivity of stoichiometric n-heptane, iso-octane, and 87 PRF in terms of exhaust CO production as a function of inlet temperatures (see Figure 4). Crank angle resolved evolution profiles of fuel, stable intermediates and oxidation products were generated for lean n-heptane (ø = 0.2 and 0.3), stoichiometric iso-octane, and stoichiometric 87 PRF at a fixed inlet temperature of 376 K. For n-heptane at ø = 0.3, the measurements were made during a cyclically repeatable two stage ignition process up to the point of hot ignition, while for n-heptane at ø = 0.2 and other fuels, species were measured during cycles where only the first stage of ignition occurred. The results have been reported [15] except for n-heptane at ø = 0.2.

The experimental results of n-heptane, iso-octane, and 87 PRF provided a basis for the model extension and validation in the current study. Besides predicting heat release, fuel consumption, and CO formation, the capability to predict the concentrations of other species classes was also a target of this work. In addition, our overall reactivity mapping results at various engine operating and inlet conditions allowed us to test the dependence of the model prediction on reaction conditions including temperature and pressure (or charge density).

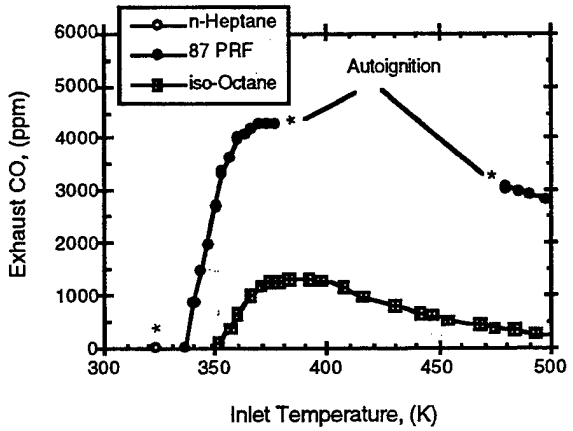

Figure 4. Exhuast CO molar fractions using stoichiometric n-hetane, iso-octane and 87 PRF at 600 rpm motored engine speed, 8.2 compression ratio, and 108.2kPa inlet pressure [15].

The specific model modifications were made mainly to (i) obtain higher specific heat release, (ii) allow prediction of other species classes, and (iii) update conjugate alkene formation submechanism. Details of the model development follow.

OBTAIN HIGHER SPECIFIC HEAT RELEASE -- As Figure 3 shows, at the end of the first stage of ignition, the previous model predicted fuel consumption higher than the experimental result. At ø = 0.3 and 376 K inlet temperature, this model predicted fuel consumption too high in comparison with experimental results even though the predicted heat release profile matched the experimental results. Thus, the model needs to be changed to obtain higher specific heat release. To this end, the oxidation paths of carbonyl radicals and olefins were modified. In the previous model, the oxidation path of carbonyl radicals is

$$O{=}R + O_2 \Leftrightarrow O{=}RO_2\cdot \quad (R1)$$

which is reaction 28 in Table 1. This produces a high concentration of $O{=}RO_2\cdot$ at the end of reaction. In reality, these large radicals oxidize to form stable species with the release of more energy. The $O{=}RO_2\cdot$ radicals can react via the following steps:

$$O{=}RO_2\cdot + O{=}RO_2\cdot \Rightarrow 2\ O{=}RO\cdot + O_2 \quad (R2)$$

$$O{=}RO\cdot \Rightarrow RCHO + RCO\cdot \quad (R3)$$

if the fuel is iso-octane, the carbonyl on the right side of R3 can be either an aldehyde or a ketone. An alternative reaction for the carbonyl radical is the direct decomposition via R4,

$$O{=}R\cdot \Rightarrow \text{Unsat. Carbonyl} + R_S\cdot \quad (R4)$$

where $R_S\cdot$ represents alkyl radicals smaller than the parent fuel. For iso-octane, the unsaturated aldehydes are methacrolein and acrolein. When the fuel is n-heptane, the unsaturated carbonyl is C=C=O. Since C=C=O has never been experimentally reported in the study of n-heptane, this path is probably not favored for this fuel.

Since the reaction paths oxidizing $R_S\cdot$ and RCO· to stable species have been included in the model, the above reactions can convert O=R· to stable species, resulting in higher specific heat release. However, this would introduce three additional reactions to the system. To reduce the number of reactions required, the result of using these steps was compared with the alternative of using a single global step:

$$O{=}R\cdot + O_2 \Rightarrow RCHO + RCO\cdot + \frac{1}{2}O_2 \quad (R5)$$

or

$$O{=}R\cdot \Rightarrow RCHO + R_S\cdot \quad (R6)$$

No significant difference in model predictions was observed. Without affecting the overall reaction rate, either R5 or R6 can even be combined with reaction 11 in Table 1, OQ'O ⇒ RCHO + O=R·, into one global step:

$$OQ'O \Rightarrow RCHO + RCHO + RCO\cdot \ -17.5\ \text{kcal/mol} \quad (R7)$$

or

$$OQ'O \Rightarrow RCHO + RCHO + R_S\cdot \ 18.5\ \text{kcal/mol} \quad (R8)$$

It should be noted that the additional O atom on the right side of R7 originates from R1. As mentioned above, R4 is not favored for n-heptane, and therefore, R7 is used for this fuel. While both R7 and R8 are possible for iso-octane, R8 gave a better result than R7. Thus, instead of pursuing the relative importance of these two pathways, R8 was selected for iso-octane in the current study. The ΔH's of R7 and R8 are derived based on the structure of the fuel molecules and the chemistry database in the HCT library [16]. As a result of these simplifications, the number of total reactions was reduced by 1.

Another approach to obtain higher specific heat release is to modify the oxidation paths of olefins. In our previous model, the olefins formed by $R_S\cdot + O_2 \Leftrightarrow C{=}C_S + HO_2\cdot$ are assumed unreactive. Model simulation shows that the concentration of $C{=}C_S$ is significantly higher than that of oxygenates, while the experimental results showed that olefins are produced in the same or lower concentration than oxygenates for iso-octane and n-heptane, respectively. As olefins have higher formation enthalpy than oxygenates, converting the extra $C{=}C_S$ into oxygenates can result in additional heat release. The oxidation of $C{=}C_S$ is assumed to follow the "Waddington" mechanism [17], as does the olefin C=C. The mechanism proposes that after addition of OH· to the C=C double bond, the resulting energetic radical -COH-C*- will be stabilized by collision with another molecule. Next, O_2 adds to the stabilized radical site forming -COH-COO·-. This is a short-lived radical which decomposes by forming a six-membered transition ring and splitting into two carbonyls and OH·. However, the oxidation paths can not be written in the same form as for C=C (reactions 26 and 27 in Table 1):

$$C{=}C_S + OH\cdot \Rightarrow \text{-OHC-Cs·-} \quad 26.5\ \text{kcal/mol} \quad (R9)$$

$$\text{-OHC-Cs·-} + O_2 \Rightarrow 2\ RCHO + OH\cdot \ -106\ \text{kcal/mol} \quad (R10)$$

The reason is that RCHO will be oxidized to form $C{=}C_S$ via reactions 19, 20 and 22 in Table 1. After each cycle the number of C atoms is reduced by 1. When RCHO becomes a formaldehyde, $C{=}C_S$ can not be formed. This process can not be handled by a reduced model without significantly increasing the number of reactions. Instead of pursuing these details, the aldehydes formed through this path are labeled as Oxy (oxygenates) and assumed unreactive. Without affecting the model performance, these two reactions can also be combined into one global reaction as R11:

$C{=}C_S + OH\cdot \Rightarrow 2\ Oxy + OH\cdot$ -76.5 kcal/mol (R11)

In addition, simulation with the model shows that the major portion of the olefins are $C{=}C_S$ formed through the smaller alkyl radicals $R_S\cdot$. For simplicity, all olefins are treated the same as $C{=}C_S$. The subscript "s" can then be removed. Thus, the number of reactions is reduced by 1. The rate parameters of R11 are selected from the work of Pitz et al. [18] assuming that $C{=}C_S$ is iso-butene.

ALLOW PREDICTION OF OTHER SPECIES CLASSES -- There are several considerations in adapting the model for prediction of other species classes. First, the experimental results show that, a major oxidation product class for PRF's is the heterocyclic ethers which can account for 30% of the fuel reacted for iso-octane and 26% for 87 PRF. Thus, it is desirable to include this reaction path. The heterocyclic ethers are formed through two steps:

$RO_2\cdot \Leftrightarrow$ QOOH-7· (R12)

QOOH-7· $\Rightarrow$ Ethers + $OH\cdot$ (R13)

the -7 in QOOH-7· designates that the ring holds seven atoms including oxygen and hydrogen atoms. For simplicity, these two reactions are combined into a global step:

$RO_2\cdot \Rightarrow$ Ethers + $OH\cdot$ -25 kcal/mol (R14)

The ΔH of R14 is selected based on the chemistry database in the HCT library [16]. For the rate parameter selection, the activation energy of R14 was taken from that of R12 in a detailed model [19] assuming the parent fuel is iso-octane, while A_{14} was set so that the yield fraction of heterocyclic ethers match the experimental results.

The second consideration is that the chain termination reaction

$R\cdot + R\cdot \Rightarrow RH$ (R15)

in the baseline model does not effectively occur, because neither C14 nor C18 species have been reported for n-heptane and iso-octane. This reaction originated from the model developed by Halstead et al. [6, 7] in which R15 is mathematically necessary to limit the reaction rate during first stage ignition. With the extended version of the model, this reaction is not necessary and is removed.

Thirdly, in the baseline model, ROOH is treated the same as OQ'OOH. For species prediction, the two species need to be differentiated, because OQ'OOH decomposes to eventually form a RCHO, an O=R· and an $OH\cdot$ while ROOH decomposes to produce a RCHO, a $R_S\cdot$ and an $OH\cdot$ via the following reactions:

$ROOH \Rightarrow RO\cdot + OH\cdot$ 43.6 kcal/mol (R16)

$RO\cdot \Rightarrow RCHO + R_S\cdot$ -10 kcal/mol (R17)

The ΔH and rate parameters of R16 are the same as those for R_SOOH in reaction 24 in Table 1. For R17, the rate parameters were selected based on the work of Westbrook and Pitz [19], while the ΔH was taken from the chemistry database in the HCT library [16].

Finally, there should be chemical paths for all radicals to convert to molecular species. Thus, reaction 29 in Table 1 was removed so as to avoid the necessity for additional reactions to convert $RCO_3\cdot$ into stable products. Such detail was not pursued in order to minimize the total number of reactions in the model.

After these modifications, all of the fuel reacted is eventually converted into CO, olefins, heterocyclic ethers, and other oxygenates, which is consistent with experimental measurements.

UPDATE CONJUGATE ALKENE FORMATION SUBMECHANISM -- In the previous model, conjugate alkenes are formed via direct H atom abstraction from alkyl radicals by an oxygen molecule, see reactions 8 and 22 in Table 1. However, recent studies [20,21] have shown that conjugate alkenes are primarily formed through coupled mechanisms:

$R\cdot + O_2 \Leftrightarrow RO_2\cdot{}^*$ (R18)

$RO_2\cdot{}^* \Rightarrow$ Olefin + $HO_2\cdot$ (R19)

$RO_2\cdot{}^* + M \Rightarrow RO_2\cdot + M$ (R20)

where $RO_2\cdot{}^*$ and M represent an energized alkylperoxide radical and any third body, respectively. For simplicity, reactions 8 and 22 in Tables 1 and 2 are replaced by the following two reactions:

$RO_2\cdot \Rightarrow C{=}C + HO_2\cdot$ 17.5 kcal/mol (R21)

$R_SO_2\cdot \Rightarrow C{=}C + HO_2\cdot$ 4 kcal/mol (R22)

The activation energy of R21 was assigned that of iso-octane using data of a detailed model [19], while A_{22} was set so that the yield fraction of conjugate alkene matched the experimental results. It was successful for iso-octane. For n-heptane, however, an A factor of R21 which matches both the yield fraction of conjugate alkenes and the overall reactivity profile could not be found. For simplicity, the A_{21} used for n-heptane and 87 PRF was taken from that for iso-octane. This resulted in underprediction of conjugate alkenes for these two fuels when their overall reactivity was matched. The ΔH of R21 was taken from the chemistry database in the HCT library [16]. The rate parameters of R22 were taken from a detailed mechanism of ethane used by Wagner et al. [22], while the ΔH for this reaction is derived from reactions 21 and 22 in Table 1. The new

conjugate alkene formation mechanism improved the sensitivity of the model to charge density.

One additional modification was the addition of R23, which is believed important for alkanes containing fewer than 4 carbon atoms. The ΔH and rate parameters were taken from reaction 17 in Table 1.

$$RH + R_SO_2\cdot \Rightarrow R_SOOH + R\cdot \quad 8\ kcal/mol \quad (R23)$$

The new version of our model is detailed in Table 2. The total number of reactions and number of active species are the same as in Li et al. [14], but the details are different. Results using this model are presented next. In the following section, the comparison between the new model and experiments is presented, along with a discussion of the rate parameters recommended for key reactions.

RESULTS WITH THE CURRENT MODEL

Two sets of experimental data were used to test and tune the model. The first set is the crank angle resolved heat release and species data at 376 K inlet temperature for lean n-heptane (ø = 0.3 and 0.2) and for stoichiometric iso-octane and 87 PRF. The second set is the exhaust CO mapping data at various inlet temperatures and compression ratios for iso-octane and 87 PRF.

The modeling procedures were described in our previous paper [14], but are briefly reviewed here. First, core temperatures and heat release are calculated from pressure data using a thermodynamic model. Secondly, the energy equation is integrated to simulate compression temperature assuming no chemical reactivity. The heat transfer coefficient is set so that the simulated temperatures match the core temperature profiles calculated from pressure data before sensible preignition heat release is observed. Figure 5 shows the example match between the pressure derived and model simulated temperature profiles at 376 K inlet temperature where detailed species data were generated for n-heptane, iso-octane and 87 PRF.

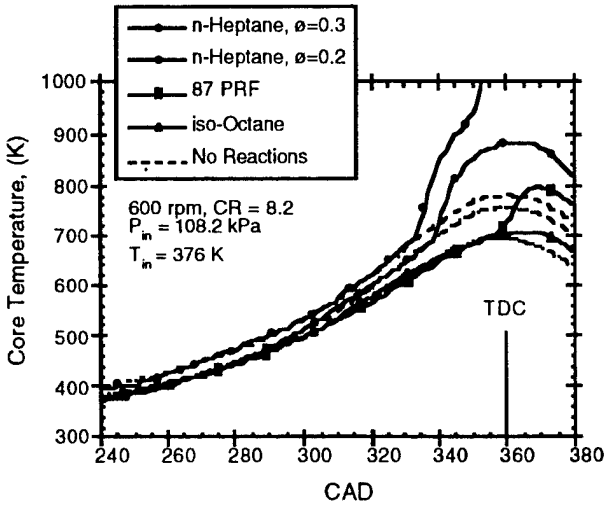

Figure 5. Core temperature profiles derived from pressure data and the temperature profiles simulated by the model assuming no reactivity.

After setting the heat transfer coefficient, the chemical kinetic rate equations and the energy equation are integrated to predict temperature and species concentrations as a function of crank angle degree.

In this study, an effort was made to account for the effects of residual gases on model prediction. Both experiments and detailed chemistry modeling have shown that the partial oxidation products in the residual gases can promote reactivity [23,24]. Westbrook et al. [25] tested the effects of pro-knock additives on the ignition time using a detailed chemical kinetic model. The tested additives include alkyl hydroperoxides, hydrogen peroxide, aldehydes, olefins, etc. It was found that the alkyl hydroperoxides are the most effective in reducing the ignition time because they can decompose to form the active radical, OH·. In the reduced model, the most important chain branching agents are OQ'OOH. Thus, the initial concentration of this species was taken into account. The procedures are as follows. First, assuming the initial charge solely consists of fuel and air, representing the first motored cycle, the concentrations of these species are calculated using the reduced model. The calculated concentration of OQ'OOH and the residual fraction (13%) were used to determine the initial concentration of these species in the next motored cycle simulation. Such procedures were repeated until the initial concentration of OQ'OOH remained unchanged.

MODELING CAD RESOLVED DATA -- The measured CAD resolved data of iso-octane, n-heptane and 87 PRF at 376 K inlet temperature were compared with model predictions. The simulation started with iso-octane. Using the parameters suggested in the baseline model, the reactivity was calculated to start later in the cycle than measured experimentally. Thus, rate parameters needed to be calibrated to match the observed induction time. In simulating knock in an engine using the Hu and Keck model [9], Cowart et al. [26] calibrated the model by reducing the activation energy of the $RO_2\cdot$ isomerization reaction (reaction 3 in Tables 1 and 2):

$$RO_2\cdot \Leftrightarrow QOOH\cdot \quad (R24)$$

from 22.4 to 21.4 kcal/mol. In addition, recent ignition delay measurements by Park et al. [27] are significantly shorter than the measurements in the Thornton rapid compression machine to which the Hu and Keck model was calibrated [9]. Thus, the rate parameters would need to be adjusted to make the reaction rate faster, which is consistent with this study. The parameter adjusted here is the activation energy of reaction 7, which was reduced from 43 to 40 kcal/mol to match the induction time of iso-octane. This parameter was selected because there is relatively high uncertainty in the original value. Another important reason for selecting this reaction is that it affects ignition delay while having only a small effect on the magnitude of the preignition heat release. The same activation energy for this reaction was used for both 87 PRF and n-heptane.

The most effective reaction in modifying the heat release profile is R25 (reaction 17 in Table 2):

$$RCHO + OH\cdot \Rightarrow RCO\cdot + H_2O \quad (R25)$$

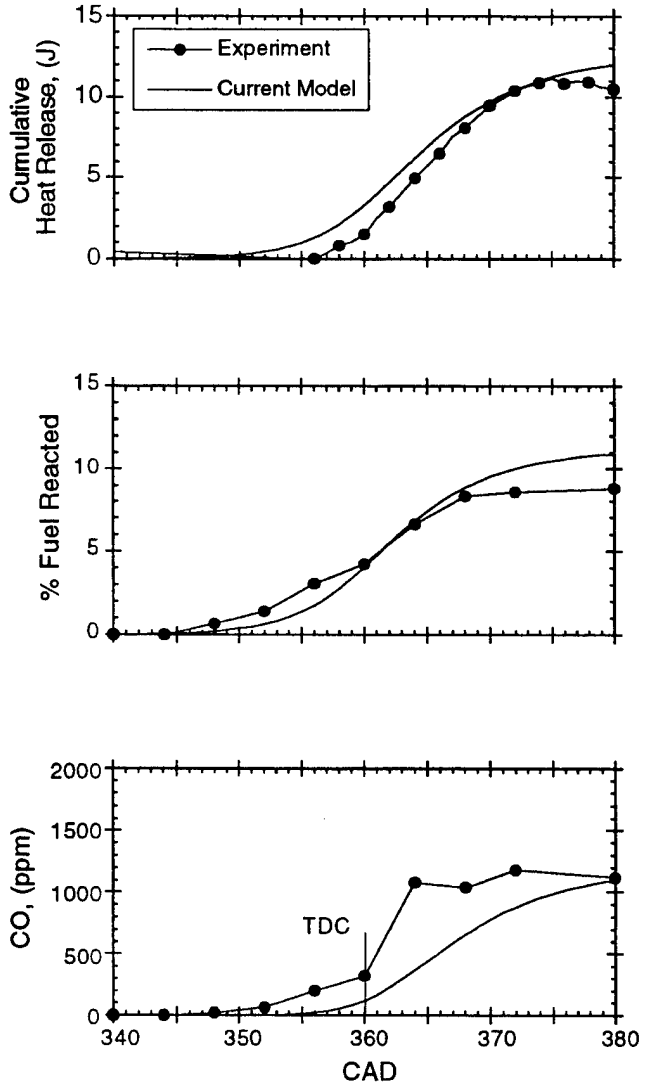

Figure 6. Comparison of heat release, fuel consumption and [CO] predictions of the current model with the experimental results of iso-octane at 8.2 compression ratio, 600 rpm, 108.2 kPa inlet pressure, and 376 K inlet temperature.

This reaction has little impact on the induction time of the first stage of ignition. The baseline rate parameters of this reaction were taken from the HCT database [16] assuming that RCHO is acetaldehyde. To match the heat release profile, A_{19} had to be set at 3.7 times the baseline value. The rationale for making this adjustment is explained shortly with the results of modeling n-heptane oxidation. For other reactions, A_{14} and A_{21} were set to match the yield fraction of heterocyclic ethers and conjugate alkenes, which are 30% and 9%, respectively.

The results of heat release, fuel consumption, and CO concentration predicted by the model, along with the experimental data, are shown in Figure 6. It can be seen that the computed profiles are quite close to the experimental results. For other species classes, the predicted concentration of oxygenates other than heterocyclic ethers is approximately the same as olefins at the end of reaction, which is consistent with experiments.

The simulated and experimental results of n-heptane at ø = 0.3 and 0.2 are presented in Figure 7. As suggested by Hu and Keck [9], the rate parameters of $RO_2\cdot$ isomerization (R24) are the major variables to account for the fuel structure effects on ignition delay. Using the same values of A_{24} and E_{24} in the baseline model, the induction times were matched for both equivalence ratios. However, the magnitude of first stage heat release was lower than in the experiments. In order to match the preignition heat release, the A_{25} was tuned to a value 1.65 times the one in the HCT database [16] assuming that RCHO is acetaldehyde. The third rate parameter adjusted was A_{14} to match the yield fraction of heterocyclic ethers. The value selected is 3.3 times that of iso-octane. With these rate parameter adjustments, the predicted profiles of heat release, fuel consumption and CO formation are close to experimental results except that the second stage ignition delay occurred 4 CAD earlier than in the experiment with ø = 0.3. Consequently, the A factor of the chain branching reaction:

$$H_2O_2 + M \Rightarrow 2\ OH\cdot + M \qquad \text{(R26)}$$

(reaction 10 in Table 2) was multiplied by 0.6 to obtain a better match of the ignition delay of the second stage ignition. The predicted and experimental results are shown in Figure 7. For other species classes, the predicted concentration of oxygenates other than heterocyclic ethers is about 30% higher than olefins at the end of the first stage but before the second stage ignition, which is again consistent with experiments.

The modeling results of n-heptane are exciting in that, with a value of A_{25} close to that of the corresponding elementary reaction, the heat release profile, fuel consumption, and CO formation at both equivalence ratios are in good agreement with experiments. However, it is necessary to justify the use of a larger A_{25} for iso-octane than n-heptane. In addition to leading to CO formation, R25 removes OH· and therefore reduces preignition reactivity. In reality, olefins may also play such a role. This is particularly true for iso-octane because its major intermediate species, iso-butene, reduces reactivity at low temperatures. However, for simplicity, the current model assumes that all olefins follow only the "Waddington" mechanism, resulting in an exclusion of this possible inhibition role. It is expected that A_{25} is similar for both n-heptane and iso-octane if the inhibition path of iso-butene is taken into account. But this would significantly increase the number of total reactions. Hence, these details were not taken into account in the current study.

For 87 PRF, only those rate parameters which are different for n-heptane and iso-octane were tuned. For R24, the activation energy for iso-octane was used for 87 PRF and A_{24} was set 4 times that of iso-octane to match the observed induction time. The A_{25} selected to match the heat release profile was 3.5 times the one in the HCT database [16] assuming that RCHO is acetaldehyde. In order to match ethers yield fraction (26%), the A_{14} used was 2.5 times that for iso-octane.

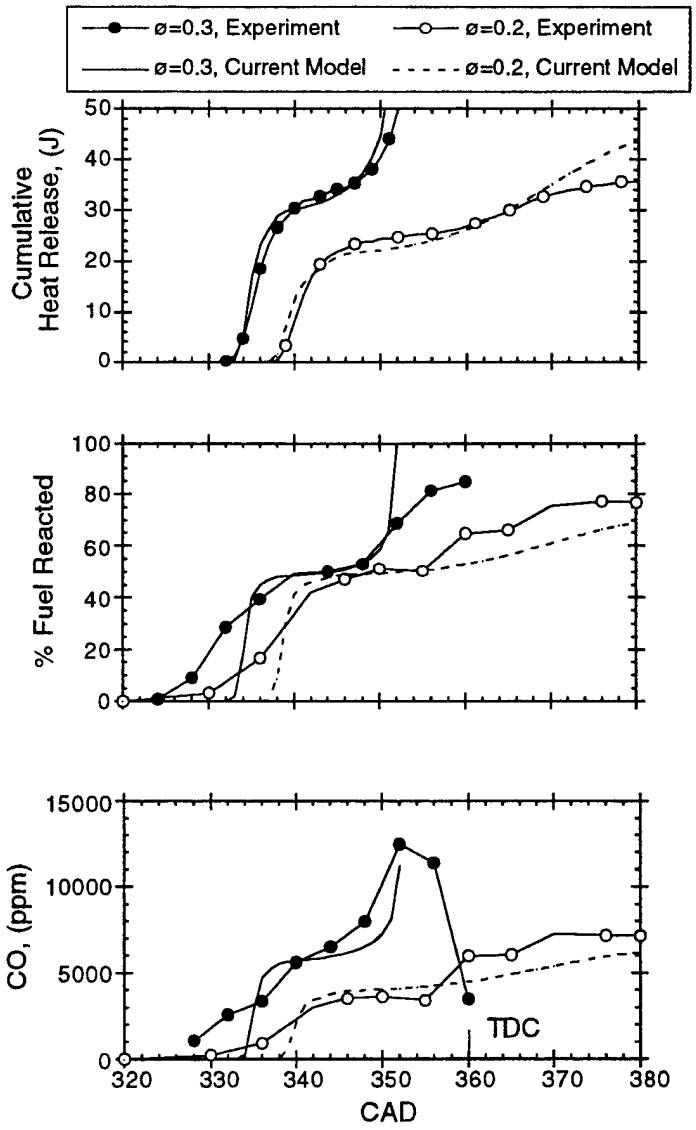

Figure 7. Comparison of heat release, fuel consumption and [CO] predictions of the current model with the experimental results of n-heptane at 8.2 compression ratio, 600rpm, 108.2 kPa inlet pressure, and 376 K inlet temperature.

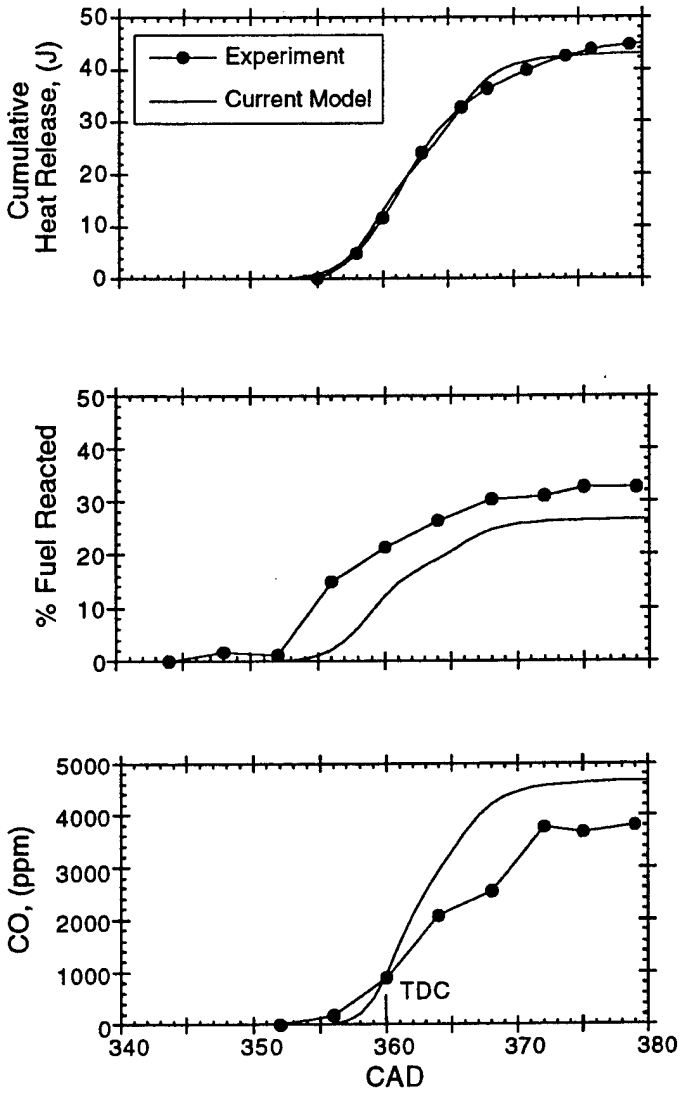

Figure 8. Comparison of heat release, fuel consumption and [CO] predictions of the current model with the experimental results of 87 PRF at 8.2 compression ratio, 600 rpm, 108.2 kPa inlet pressure, and 376 K inlet temperature.

The results of heat release, fuel consumption, and CO concentration predicted by the model, along with the experimental data, are shown in Figure 8. The heat release profile is matched very well, but, the CO and fuel consumption differ from the experiments by approximately 20%. For other species classes, the predicted concentration of oxygenates other than heterocyclic ethers is about 20% higher than olefins at the end of reaction, while the experimental results show that the former is about 80% higher than the latter. Thus, the species prediction for 87 PRF is not as good as for the neat PRF's.

The above predictions were conducted at one inlet condition. The performance of the model at other engine operation conditions is examined next.

MODELING AT VARIOUS ENGINE CONDITIONS -- The major physical factors affecting oxidation reactivity at low and intermediate temperatures are temperature and pressure (or charge density). It is important that the model has the ability to account for the effects of these factors.

As shown in Figure 4, as the inlet temperature was increased, the reactivity of iso-octane first increased, followed by a plateau, and then decreased, exhibiting a negative temperature coefficient (NTC) behavior. No autoignition occurred. The reactivity of 87 PRF was much higher than iso-octane, but its profile as a function of temperature is similar to iso-octane. Sporadic autoignition (two stage ignition) was observed as the inlet temperature was increased to 377 K. However, when the inlet temperature reached 480 K, autoignition ceased. As the inlet temperature was further increased to 500 K, autoignition still did not occur and exhaust CO was further decreased. This observation suggests that the reactivity or magnitude of preignition reaction has a significant effect on the second stage of ignition.

The existing general hydrocarbon oxidation mechanism can explain the NTC behavior in terms of a

shift of $RO_2\cdot$ reaction mechanism to alkene formation paths. This mechanism is included both in the baseline model and in the extended reactions. Thus, the model can at least qualitatively account for the effects of temperature. The ability of the model to quantitatively predict the NTC behavior was tested using the overall reactivity mapping results presented in Figure 4.

As to the pressure effects, experiments show that preignition reactivity increases as the pressure (or charge density) increases. Benson [28] qualitatively analyzed the effects of pressure on the temperature at which the $RO_2\cdot$ shift from degenerate chain branching paths to conjugate alkene formation paths. The analysis is based on the following reactions:

$$R\cdot + O_2 \Leftrightarrow RO_2\cdot \qquad \text{(R27)}$$

$$RO_2\cdot + RH \Rightarrow ROOH + R\cdot \qquad \text{(R28)}$$

$$R\cdot + O_2 \Rightarrow C{=}C + HO_2\cdot \qquad \text{(R29)}$$

Based on the steady-state analysis and assuming that $RO_2\cdot$ and $R\cdot$ are in equilibrium via R27, the rates of production of ROOH and the olefin is developed and found to give the ratio

$$\frac{d[C{=}C]}{d[ROOH]} = \frac{k_{29}}{k_{28}\,k_{27}\,[RH]} \qquad (1)$$

Thus, at the same temperature, when the charge density is increased, the concentration of the fuel [RH] is increased and the formation of ROOH is favored, resulting in higher reactivity. Since ROOH is a major chain branching agent for light HC's, equation (1) applies for light HC's only. For larger HC's like PRF's, the major chain branching paths are through R24. The charge density does not directly affect the competition between chain branching agent formation and olefin formation. Thus, the baseline model has a relatively weak dependence of reactivity on charge density. For $R_S\cdot$ reactions in the previous model, however, Benson's analysis applies. With the updated conjugate formation path R22 in the current model, the rate of production of R_SOOH and the olefin is

$$\frac{d[C{=}C_s]}{d[R_sOOH]} = \frac{k_{22}}{k_{23}\,[RH]} \qquad (2)$$

It should be noted equation (2) holds without the assumption of the equilibrium between $RO_2\cdot$ and $R\cdot$. Thus, the extended reactions in the current model improve the pressure dependence of the model.

To test the model's sensitivity to pressure, or charge density, an exhaust CO mapping of 87 PRF at CR = 5.2 was also compared with model predictions. In that experiment, the engine was operated at 900 rpm, 165 kPa with inlet pressure and the charge density at top dead center (TDC) being about 15% lower that at CR = 8.2.

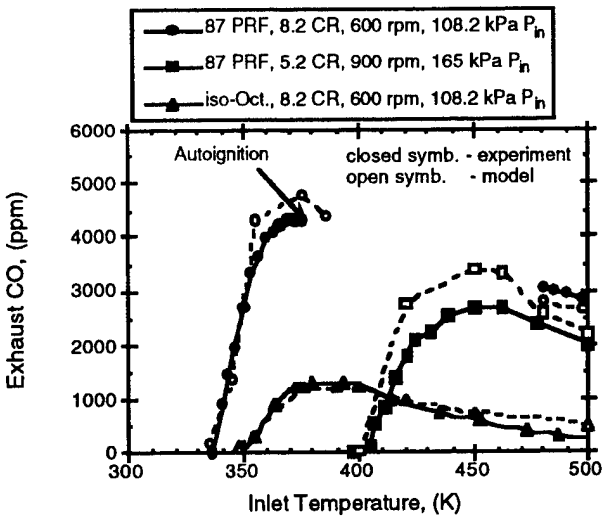

Figure 9. Comparison of the exhaust CO predictions of the current model with the experimental results of 87 PRF and iso-octane at various engine conditions.

The experimental results and model predictions are presented in Figure 9. It can be seen that the NTC behavior of iso-octane and 87 PRF were reproduced. The predicted dependence of reactivity on pressure, or charge density of 87 PRF was also in agreement with experiments.

During the reactivity test of 87 PRF, sporadic autoignition was observed experimentally at inlet temperatures between 377 and 480 K, while the model predicted no autoignition using the averaged initial parameters. It is desirable that the sporadic autoignition phenomena be interpreted by the reduced model. In this regard, the causes for this phenomena were analyzed in order to identify the initial parameters which need to be changed for modeling the autoignition cycle. From the pressure traces, it was observed that there is no apparent reactivity, or heat release in the cycle before an autoignition cycle. The model simulation shows that for a cycle at the transition state from minimal to significant reactivity, the level of OQ'OOH can be up to hundreds of ppm. On the other hand, for cycles with significant reactivity, the simulated concentration of OQ'OOH is only about 0.5 ppm. Thus, it is highly likely that the "non-reactivity" cycle provided a high concentration of active species which promoted reactivity and produced autoignition in the next cycle. This hypothesis is supported by the experimental work of Walcutt et al. [29], in which they found that the thermoneutral reactions occurring prior to the onset of cool flames result in the decrease in the anti-knock performance of the fuel.

Following the above analysis, the initial level of OQ'OOH in the model was gradually increased at the inlet temperature of 377 K, where autoignition was first experimentally observed. The simulation predicted autoignition when the initial level of OQ'OOH reached 130 ppm. This indicated that if the "non-reactivity" cycle produces 1000 ppm OQ'OOH, which is possible, the next cycle will autoignite. Using the same level OQ'OOH, the model did not predict autoignition for

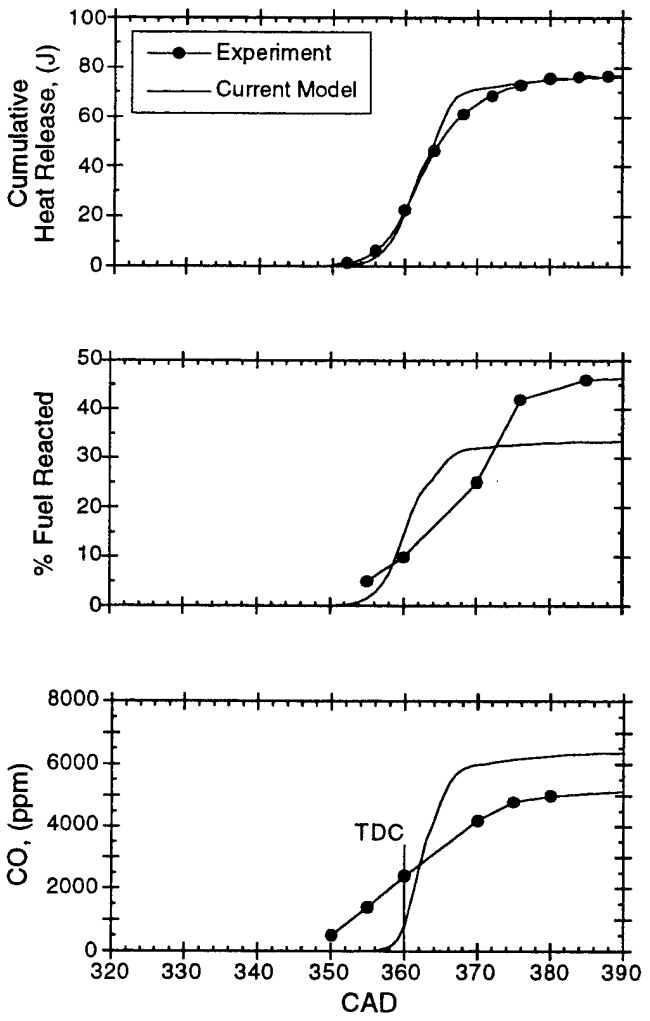

Figure 10. Comparison of the heat release, fuel consumptions and CO predictions of the current model with the experimental data of 63 PRF at 5.2 compression ratio, 900 rpm, 165 kPa inlet pressure, and 445 K inlet temperature.

87 PRF at lower temperatures nor autoignition of iso-octane at any temperature, which is consistent with experiments. Thus, this sporadic autoignition of 87 PRF can be interpreted by the reduced model. However, due to the uncertainties in the initial level of OQ'OOH, a quantitative prediction on the inlet temperature range where autoignition occurred is impossible.

Since significant modifications have been made to our previous model, it is prudent to test the current model against the experimental results of 63 PRF presented in Figure 3. Following the same method for modeling 87 PRF, A_{24} was set to match induction time, while A_{25} was set to match the magnitude of heat release. Since the hetrocyclic ethers were not reported for that fuel, the value of A_{14} was assigned by a RON based linear interpolation using the A_{14}'s of n-heptane and 87 PRF. The final value of A_{24} is 9.5 times that of iso-octane, while A_{25} is 2.7 times that in the HCT database [16] assuming that RCHO is acetaldehyde. The results of heat release, fuel consumption, and CO concentration predicted by the model, along with the experimental data, are shown in Figure 10. It can be seen that the predicted heat release profile is much improved compared with Figure 3. The fuel consumption and CO predictions differ from experiments by about 22 and 25%, respectively. It is also observed that the problem with continued CO formation at late CAD's predicted by the previous model disappears.

DISCUSSION

Table 2 represents the final reduced mechanism and recommended rate parameters, including the modifications necessary to accommodate different fuels structure. As expected, the fuel specific parameters change monotonically with the octane number of the fuels. In addition, using the rate parameters developed based on the CAD resolved measurements at one inlet engine condition, the model reproduced the complicated oxidation behavior at various engine inlet and operating conditions. This behavior indicates that the modification of these rate parameters was not just an empirical exercise, but one that captured the essence of the underlying chemical processes.

In comparison with other reduced models, two improvements were made with the current model:

(1) The mechanisms (primarily via secondary reactions) necessary to account for preignition heat release have been included.

(2) All of the fuel reacted is eventually converted to molecular oxidation products which can be divided into CO, olefins, heterocyclic ethers and other oxygenates.

Under the experimental conditions examined, the model predictions agreed fairly well with experiments. Nonetheless, there are a number of factors that must be considered prior to full utilization of this model for engine applications. First, the model needs to be tested under broader engine conditions, particularly at higher pressures and higher engine speed, so that the fuel/air mixture experiences conditions closer to those of the end gas in fired engines.

Second, the number of reactions needs to be optimized. Existing reduced models consist of reactions ranging from a few to nearly a hundred. From the viewpoint of engine applications, a model with the sufficient prediction ability and the smallest number of reactions is desirable. The issue regarding this trade-off remains unaddressed, and definitely deserves additional effort. We feel that there is a potential for reducing the number of reactions in the current model without significantly affecting its predictions.

Third, the model needs to be adapted for a broader range of fuels. Since most paraffins follow similar chemical pathways, the present model developed for PRF's can be conveniently adapted to other paraffins. However, in order to develop a model for practical fuels, the model needs to be extended to include initiation steps for olefins, aromatics, oxygenates and their mixtures.

SUMMARY AND CONCLUSIONS

We developed a reduced chemical kinetic model for the prediction of major oxidation behavior of PRF's at low and intermediate temperatures, including ignition delay, preignition heat release, fuel consumption, CO formation and production of other species classes. The model development was carried out in two phases. In the first phase, which was previously reported [14], an existing reduced ignition model of 18 reactions and 13 active species was extended to account for specific heat release and CO formation, ending up with 7 new active species and 11 additional reactions. This model was tuned to match the experimental results of a 63 PRF, at one engine operating condition.

In the second phase, the model was modified utilizing n-heptane, iso-octane and 87 PRF experimental data from our recent motored engine study of PRF autoignition chemistry [15]. Modifications primarily included the refinement of carbonyl and olefin reactions for higher specific heat release, incorporation of reaction paths to generate key classes of species, and updating the conjugate alkene formation submechanism. The total number of active species and reactions remains the same as the initially extended model, but with different details. Accommodating the different fuels requires mainly adjusting the rate parameters of the $RO_2\cdot$ isomerization reaction, the reaction of aldehydes with $OH\cdot$, and the reaction of forming cyclic ethers for each fuel.

At the motored engine condition where detailed species data were generated, the model can reproduce the ignition delay and the magnitude of the preignition heat release. Fuel consumption and CO formation predictions differed from experiments by at most 25% for all of the four fuels. Predictions for other species classes generally agreed with experiments. The overall reactivity measurements at various inlet conditions were also used to test the dependence of the model predictions on temperature and charge density. The NTC behavior of iso-octane and 87 PRF was reproduced by the model. In addition, the lower reactivity of 87 PRF at a lower compression ratio was also reproduced, indicating that the model can account for the effects of pressure or charge density.

These results indicated that the current reduced kinetic model is a useful tool for prediction of major oxidation behavior at low and intermediate temperatures.

ACKNOWLEDGEMENTS

This research was supported by the U.S. Department of Energy, Office of Transportation Technologies under Contract No. DE-FG04-87AL44658, and by the U.S. Army Research Office under Grant No. DAAH04-93-G-0042.

REFERENCES

1. Dryer, F.L., "The Phenomenology of Modeling Combustion Chemistry", Fossil Fuel Combustion - A Source Book, W. Bartok and A.F. Sarofim, eds.; John Wiley and Sons, Inc., 1991.

2. Vermeersch, M.L., Held, T.J., Stein, Y. and Dryer, F.L., "Autoignition Chemistry Studies of n-Butane in a Variable Pressure Flow Reactor", SAE Paper No. 912316, SAE Trans., Section 4, 1991.

3. Gluckstein, M.E. and Walcutt, C., "End-Gas Temperature-Pressure Histories and Their Relation to Knock", SAE Trans., 69, 1964.

4. Smith, J.R., Green, R.M., Westbrook, C.K., and Pitz, W.J., "Experimental and Modeling Study of Engine Knock", Twentieth Symposium (International) on Combustion, p. 91, The Combustion Institute, Pittsburgh, 1984.

5. Griffiths, J.F., "Reduced Kinetic Models and Their Application to Practical Combustion Systems", Prog. Energy Combust. Sci. 21, 25, 1995.

6. Halstead, M.P., Kirsch , L.J., Prothero, A. and Quinn, C.P., "A Mathematical Model for Hydrocarbon Autoignition at High Pressure", Proc. Roy. Soc., A346, 515, 1975.

7. Halstead, M.P., Kirsch , L.J., Prothero, A. and Quinn, C.P., "The Autoignition of Hydrocarbon Fuels at High Temperatures and Pressure - Fitting of a Mathematic Model", Combustion and Flame, 30, 45, 1977.

8. Cox, R.A. and Cole, J.A., "Chemical Aspects of the Autoignition of Hydrocarbon/Mixtures", Combustion and Flame, 60, 109, 1985.

9. Hu, H. and Keck, J., "Autoignition of Adiabatically Compressed Combustible Gas Mixtures", SAE Paper No. 872110, SAE Trans., 91, 1987.

10. Griffiths, J.F., Hughes, K.J., Schreiber, M., and Poppe, C., "A Unified Approach to the Reduced Kinetic Modeling of Alkane Combustion", Combust. and Flame, 99, p. 533, 1994.

11. Kalghatgi, G.T., Snowdon, P. and McDonald, C.R., "Studies of Knock in a Spark Ignition Engine with 'CARS' Temperature Measurements and Using Different Fuels", SAE paper No. 950690, 1995.

12. Leppard, W.R., "The Autoignition Chemistry of Primary Reference Fuels, Olefin/Paraffin Binary Mixtures, and Non-Linear Octane Blending", SAE Paper No. 922325, SAE Trans., Section 4, 1992.

13. Filipe, D.J., Li, H., Miller, D.L. and Cernansky, N.P., "The Reactivity Behavior of n-Heptane and Isooctane Blends in a Motored Knock Research Engine", SAE Paper No. 920807, 1992.

14. Li, H., Miller, D.L., and Cernansky, N.P., "A Study on the Application of a Reduced Chemical Reaction Model to Motored Engines for Heat Release Prediction", SAE Paper No. 922328, SAE Trans., Section 5, 1992.

15. Li, H., Prabhu, S.K., Miller, D.L., and Cernansky, N.P., "Autoignition Chemistry Studies on Primary Reference Fuels in a Motored Engine", SAE Paper No. 942062, SAE Trans.,1994.

16. Lund, C.M., "HCT - A General Computer Program for Calculating Time - Dependent Phenomena Involving One - Dimensional Hydrodynamics, Transport, and Detailed Chemical Kinetics", LLNL Report UCRL - 52504, Lawrence Livermore National Laboratory, Livermore, CA, 1989.

17. Ray, D.J.M. and Waddington, D.J., "Gas Phase Oxidation of Alkenes - Part II. The Oxidation of 2-Methylbutene-2 and 2,3-Dimethylbutene-2", Combust. and Flame, 21, 327, 1973.

18. Pitz, W.J., Westbrook, C.K., and Leppard, W.R.,, "Autoignition Chemistry of C4 Olefins Under Motored Engine Conditions: A Comparison of Experimental and Modeling Results", SAE paper 912315, SAE Trans., Section 4, 1991.

19. Westbrook, C.K. and Pitz, W.J., "A Chemical Kinetic Mechanism for the Oxidation of Paraffinic Hydrocarbons Needed for Primary Reference Fuels", Paper No. WSSCI 93-011, presented at the Spring Meeting of the Western States Section/The Combustion Institute, Salt Lake City, UT, 22-23 March, 1993.

20. Slagle, I.R., Feng, Q., and Gutman, D., "Kinetics of the Reaction of Ethyl Radicals with Molecular Oxygen from 294 K to 1002 K", J. Phys. Chem., Vol. 88, p. 3648, 1984.

21. Slagle, I.R., Park, J.-Y., and Gutman, D., "Experimental Investigation of Kinetics and Mechanism of the Reaction of n-Propyl Radicals with Molecular Oxygen from 297 to 635 K", Twentieth Symposium (International) on Combustion, p. 733, The Combustion Institute, Pittsburgh, 1984.

22. Wagner, A.F., Slagle, I.R., Sarzynski, D. and Gutman, D., "Experimental and Theoretical studies of the $C_2H_5 \cdot + O_2$ Reaction Kinetics", J. Phys. Chem., Vol. 94, 1990.

23. Levedahl, W.J. and Howard, F.L., "Two-stage Autoignition of Some Hydrocarbons", Ind. and Eng. Chem., 43, 2805, 1951.

24. Wilk, R.D., Pitz, W.J., Westbrook, C.K., Addagarla, S., Miller, D.L., Cernansky, N.P. and Green, R.M., "Combustion of n-Butane and iso-Butane in an Internal Combustion Engine: A Comparison of Experimental and Modeling Results", Twenty-Third Symposium (International) on Combustion, p.1047, The Combustion Institute, Pittsburgh, 1990.

25. Westbrook, C.K., Pitz, W.J., and Leppard, W.R., "The Autoignition Chemistry of Paraffinic Fuels and Pro-Knock and Anti-Knock Additives: A Detailed Chemical Kinetic Study", SAE Paper No. 912314, SAE Trans., Section 4, 1991.

26. Cowart, J.S., Keck, J.C., Heywood, J.B., Westbrook, C.K. and Pitz, W.J., "Engine Knock Predictions Using a Fully-Detailed and a Reduced Chemical Kinetic Mechanism", Twenty-Third Symposium (International) on Combustion, p. 1055, The Combustion Institute, Pittsburgh, 1990.

27. Park, P. and Keck, J.C., "Rapid Compression Machine Measurements of Ignition Delays for Primary Reference Fuels", SAE Paper No. 900027, 1990.

28. Benson, S.W., "The Kinetics and Thermochemistry of Chemical Oxidation with Application to Combustion and Flames", Prog. Energy Combust. Sci. 7, 125, 1981.

29. Walcutt, C., Mason, J.M. and Rifkin, E.B., "Effect of Preflame Oxidation Reactions on Engine Knock", Ind. and Eng. Chem., 46, No. 5, 1029, 1954.

Table1

Previous Reduced Chemical Kinetic Model
Part I: The Baseline Model [9]

A. 13 Active Species

1.	RH	2.	O_2	3.	R·	4.	RO_2·	5.	QOOH·
6.	OOQOOH·	7.	OQ'O·	8.	OH·	9.	HO_2·	10.	HOOH
11.	OQ'OOH	12.	RCHO	13.	C=C				

B. 18 Reactions (unit: cc, mole, s, kcal)

Arrhenius parameters of rate constants $k = A\, e^{-E/RT}$ for heptane at 600 K < T < 1100 K

			Equilibrium		k^+		k^-	
Reaction		ΔH^0_{300}	log A	E	log A^+	E^+	log A^-	E^-
1	RH + O_2 ⇒ R· + HO_2·	46.4	1.5	46.0	13.5	46.0	12.0	0.0
2	R· + O_2 ⇔ RO_2·	-31.0	-1.4	-27.4	12.0	0.0	13.4	27.0
3	RO_2· ⇔ QOOH· (n-heptane)	7.5	0.9	8.0	11.9	19.0	11.0	11.0
	(iso-octane)	7.5	0.0	11.4	11.0	22.4	11.0	11.0
4	QOOH· + O_2 ⇔ OOQOOH·	-31.0	-1.9	-27.4	11.5	0.0	13.4	27.4
5	OOQOOH· ⇒ OQ'OOH + OH·	-26.6			11.3	17.0		
6	OH· + RH ⇒ H_2O + R·	-23.5			13.3	3.0		
7	OQ'OOH ⇒ OQ'O· + OH·	43.6			15.6	43.0		
8	R· + O_2 ⇔ C=C + HO_2·	-13.5	0.0	-13.5	11.5	6.0	11.5	19.5
9	HO_2· + HO_2· ⇒ HOOH + O_2	-38.5			12.3	0.0		
10	HOOH + M ⇒ 2OH· + M	51.4			17.1	46.0		
11	OQ'O· ⇒ RCHO + O=R·	8.5			14.0	15.0		
12	QOOH· ⇒C=C + RCHO + OH·	-3.0			14.4	31.0		
13	RO_2· + RCHO ⇒ ROOH + RCO·	-0.6			11.45	8.6		
14	HO_2· + RCHO ⇒ HOOH + RCO·	-0.6			11.7	8.64		
15	C=C + HO_2· ⇒ Epox + OH·	-0.23			10.95	10.0		
16	HO_2· + RH ⇔ R· + HOOH	8.0	0.9	8.0	11.7	16.0	10.8	8.0
17	RO_2· + RH ⇔ ROOH + R·	8.0	1.1	8.0	11.2	16.0	10.1	8.0
18	R· + R· ⇒ RH	-85.0			13.2	0.0		

Note: ROOH and OQ'OOH are treated as identical; O=R·, RCO· and Epox are assumed inactive.

Table1 (cont.)

Previous Reduced Chemical Kinetic Model

Part II: Extended Reactions [14]

A. 7 Active Species

1. RCO· 2. R_S· 3. R_SO_2· 4. R_SOOH 5. R_SO· 6. -OHC-C·- 7. RCO_3·

B. 11 Reactions (unit: cc, mole, s, kcal)

Arrhenius parameters of rate constants $k = A\, e^{-E/RT}$

			Equilibrium		k^+		k^-	
	Reaction	ΔH^0_{300}	log A	E	log A^+	E^+	log A^-	E^-
19	RCHO + OH· ⇒ RCO· + H_2O	-33.5			12.62	0.52		
20	RCO· + M ⇒ R_S· + CO + M	8.7			16.78	15.0		
21	R_S· + O_2 ⇔ R_SO_2·	-31.0	-1.4	27.4	12.0	0.0	13.4	27.0
22	R_S·+ O_2 ⇔ $C{=}C_S$ + HO_2·	-13.5	0.0	13.5	11.5	6.0	11.5	19.5
23	RCHO + R_SO_2· ⇒ R_SOOH + RCO·	-0.6			11.45	8.6		
24	R_SOOH ⇒ R_SO· + OH·	43.6			15.6	43.0		
25	R_SO· + O_2 ⇒ R_S'O + HO_2·	-26.5			10.6	2.14		
26	C=C + OH· ⇒ -OHC-C·-	26.5			12.68	- 0.79		
27	-OHC-C·- + O_2 ⇒ 2 RCHO + OH·	-106.0			10.0	-4.0		
28	O=R· + O_2 ⇔ $O{=}RO_2$·	-31.0	-1.9	-27.4	11.5	0.0	13.4	27.4
29	RCO· + O_2 ⇔ RCO_3·	-31.0	-1.9	-27.4	11.5	0.0	13.4	27.4

Note: R_S'O and $C{=}C_S$ are assumed inactive.

Table 2

Current Reduced Chemical Kinetic Model -- Part 1

A. 13 Active Species

1.	RH	2.	O_2	3.	R·	4.	RO_2·	5.	QOOH·
6.	OOQOOH·	7.	OQO·	8.	OH·	9.	HO_2·	10.	HOOH
11.	OQ'OOH	12.	RCHO	13.	C=C				

B. 16 Reactions (unit: cc, mole, s, kcal)

Arrhenius parameters of rate constants $k = A\, e^{-E/RT}$ for heptane at 600 K < T < 1100 K

			Equilibrium			k^+		k^-	
Reaction		ΔH^0_{300}	log A	E	log A^+	E^+	log A^-	E^-	
1	$RH + O_2 \Leftrightarrow R· + HO_2·$		46.4	1.5	46.0	13.5	46.0	12.0	0.0
2	$R· + O_2 \Leftrightarrow RO_2·$		-31.0	-1.4	-27.4	12.0	0.0	13.4	27.4
3	$RO_2· \Leftrightarrow$ QOOH·	n-heptane	7.5	0.9	8.0	11.9	19.0	11.0	11.0
		63 PRF	7.5	0.98	11.24	11.98	22.4	11.0	11.0
		87 PRF	7.5	0.59	11.24	11.59	22.4	11.0	11.0
		iso-octane	7.5	0.0	11.24	11.0	22.4	11.0	11.0
4	$QOOH· + O_2 \Leftrightarrow$ OOQOOH·		-31.0	-1.9	-27.4	11.5	0.0	13.4	27.4
5	$OOQOOH· \Rightarrow OQ'OOH + OH·$		-26.6			11.3	17.0		
6	$OH· + RH \Rightarrow H_2O + R·$		-23.5			13.3	3.0		
7	$OQ'OOH \Rightarrow OQ'O· + OH·$		43.6			15.6	40.0		
8	$HO_2· + HO_2· \Rightarrow HOOH + O_2$		-38.5			12.3	0.0		
9	$HOOH + M \Rightarrow 2OH· + M$		51.4			16.88	46.0		
10	$OQ'O· \Rightarrow$ 2 RCHO + RCO· (n-heptane)		-17.5			14.0	15.0		
	$\Rightarrow$ 2 RCHO + R_S· (iso-octane, 63, and 87 PRF)		18.5			14.0	15.0		
11	$QOOH· \Rightarrow$ C=C + RCHO + OH·		-3.0			14.4	31.0		
12	$RO_2· + RCHO \Rightarrow ROOH + RCO·$		-0.6			11.45	8.6		
13	$HO_2· + RCHO \Rightarrow HOOH + RCO·$		-0.6			11.7	8.64		
14	$C=C + HO_2· \Rightarrow$ Epox + OH·		-0.23			10.95	10.0		
15	$HO_2· + RH \Leftrightarrow R· + HOOH$		8.0	0.9	8.0	11.7	16.0	10.8	8.0
16	$RO_2· + RH \Leftrightarrow ROOH + R·$		8.0	1.1	8.0	11.2	16.0	10.1	8.0

Table 2 (cont.)

Current Reduced Chemical Kinetic Model -- Part 2

A. 7 Active Species

1. $RCO\cdot$ 2. $R_s\cdot$ 3. $R_sO_2\cdot$ 4. R_sOOH 5. $R_sO\cdot$ 6. $RO\cdot$ 7. $ROOH$

B. 13 Reactions (unit: cc, mole, s, kcal)

Arrhenius parameters of rate constants $k = A\, e^{-E/RT}$

			Equilibrium		k^+		k^-	
	Reaction	ΔH^0_{300}	log A	E	log A^+	E^+	log A^-	E^-
17	$RCHO + OH\cdot \Rightarrow RCO\cdot + H_2O$							
	(n-heptane)	-31.5			13.22	0.0		
	(63 PRF)	-31.5			13.43	0.0		
	(87 PRF)	-31.5			13.55	0.0		
	(iso-octane)	-31.5			13.57	0.0		
18	$RCO\cdot + M \Rightarrow R_s\cdot + CO + M$	10.7			16.78	15.0		
19	$R_s\cdot + O_2 \Leftrightarrow R_sO_2\cdot$	-31.0	-1.4	-27.4	12.0	0.0	13.4	27.4
20	$R_sO_2\cdot \Rightarrow C{=}C + HO_2\cdot$	17.5			11.75	28.9		
21	$RCHO + R_sO_2\cdot \Rightarrow R_sOOH + RCO\cdot$	-0.6			11.53	8.6		
22	$RH + R_sO_2\cdot \Leftrightarrow R_sOOH + R\cdot$	8.0	1.18	8.0	11.28	16.0	10.1	8.0
23	$R_sOOH \Rightarrow R_sO\cdot + OH\cdot$	43.6			15.6	43.0		
24	$R_sO\cdot + O_2 \Rightarrow R_s'O + HO_2\cdot$	-26.5			10.6	2.14		
25	$C{=}C + OH\cdot \Rightarrow 2\ OXY + OH\cdot$	-75.5			12.72	- 1.04		
26	$ROOH \Rightarrow RO\cdot + OH\cdot$	43.6			15.6	43.0		
27	$RO\cdot \Rightarrow R_s\cdot + RCHO$	-10.0			13.3	15.0		
28	$RO_2\cdot \Rightarrow C{=}C + HO_2\cdot$	4.0			9.85	23.0		
29	$RO_2\cdot \Rightarrow$ ether + $OH\cdot$ (n-heptane)	-25.0			9.48	18.0		
	(63 PRF)	-25.0			9.28	18.0		
	(87 PRF)	-25.0			9.18	18.0		
	(iso-Octane)	-25.0			8.78	18.0		